Analysis of experimental scattering sources in local ductility measurement from flat tensile test sample fracture surfaces

Patrick Larour[1*], *Wolfgang* Lumetzberger[1], and *Leopold* Wagner[1]

[1]voestalpine Stahl GmbH, R&D Forming Technologies, voestalpine-Str. 3, 4020 Linz, Austria

Abstract. Local formability measurement from fracture surfaces out of flat sheet tensile test samples is increasingly gaining momentum for AHSS automotive sheet steel grades characterization. A newly released VDA 238-110 test standard specifies the experimental methods and addresses the particular testing challenges with focus on reduction of area and thickness reduction at minimum fracture thickness from postmortem microscope measurements on tensile testing sample fracture surfaces. The scattering of testing results depends on the one hand on the measuring challenges when dealing with a broad variety of fracture shapes. On the other hand, systematic geometric effects such as sample width to thickness w/t ratio typically between ISO, ASTM or JIS tensile sample geometries also play a key role. The w/t ratio influences largely the fracture angle in width direction and fracture morphology in thickness direction and subsequently the overall local ductility level. This issue is discussed with two common cold rolled AHSS steel grades DP800 and CP1000 with large w/t ratio variations. Local formability material testing can be interpreted satisfyingly by sorting out stochastic test result variations within a stable fracture angle region separately from the systematic low vs. high fracture angle regions offset.

Keywords: AHSS; Local ductility; Test scattering; VDA 238-110.

1 Introduction

Determining tensile test based local ductility has gained interest over the last years. A dedicated VDA 238-110 testing standard for flat sheet testing and microscope fracture image analysis has recently been released based on a large round robin test within the European steel and automotive industry [1]. The area reduction at fracture as well as thickness reduction based on minimum thickness in tensile sample shape are both outputs of this standard. Round robin results (18 labs, 1500 tests) show a significant smaller scattering as compared to ISO16630 hole expansion ratio, with reproducibility and repeatability of testing results roughly in the same order of magnitude as for the tensile total elongation [2].

The work of Hance [3-7] first illustrates the usefulness of local-global formability plots on the basis of reduction of area and derived true fracture strain for flat sheet samples as summarized in WorldautoSteel guidelines [3]. Applications with regard to material classification by means of formability and performance index as well as local/global strain ratio are proposed in [4-6]. Correlations with stretch flangeability [6, 7] also show the broad range of application of this concept.

Another testing method is propagated by the work of Heibel et al. [8] rather focusing on simpler thickness reduction at minimum thickness within fracture area. This method is currently rather favored by OEM's.

Tensile local formability investigations performed at voestalpine [9-13] focus on experimental testing issues and sample geometry influence both for standard [9,10] and notched samples [11] and applicability to stretch flangeability prediction [12,13]. The fracture angle in width and ductile/shear fracture type in thickness direction depend heavily on sample geometry (i.e. width to thickness ratio). Those parameters are contributing to result variability.

Some mixed DIC/FEM testing method with local thickness correction method has been explored by other authors, as usually practiced for Forming Fracture Line determination from FLC samples [14,15].

Reasonable correlations between local ductility (tensile thickness & area reduction at fracture) and edge crack sensitivity (ISO16630 punched hole expansion ratio) have been reported for cold AHSS steels in several independent investigations [6-8,12,15]. However contradicting data suggest especially for hot rolled steels a weak to non-existing correlation between local ductility and edge crack formability [16-18]. This tempers initial high expectations about tensile test-based correlations with stretch flangeability.

The aim of this work is to show the experimental challenges related to tensile local formability measurement for microscope-based thickness and area measurement on broken tensile test samples according to VDA 238-110, with a special focus on sample geometry and fracture morphology interactions with local formability measurements.

* Corresponding author: patrick.larour@voestalpine.com

2 Experimental testing issues

Local ductility measurements on fractured tensile test samples present significant challenges. In this chapter random cold and hot rolled AHSS sheet steels are used for illustration from own testing database in the tensile strength 600-1200MPa and 1-4mm thickness range.

The fracture angle - typically between 0 and 35° - is defined hereafter to be identical to the tilting angle necessary to optimally position the fracture surface horizontally under microscope as explained in [1, 10].

2.1 Tensile sample failure location

Fig. 1 illustrates for different fracture angles the relative position of minimum thickness at fracture (yellow line which is extended as dotted red line) versus crack initiation location assumed at the point of widest opening gap in the lateral view between both broken sample parts around sample center. The minimum thickness is often not located at sample center as illustrated in Fig. 1 for 15-30° fracture angle. This raises some questions about the physical meaning of minimum absolute thickness versus thickness at sample center.

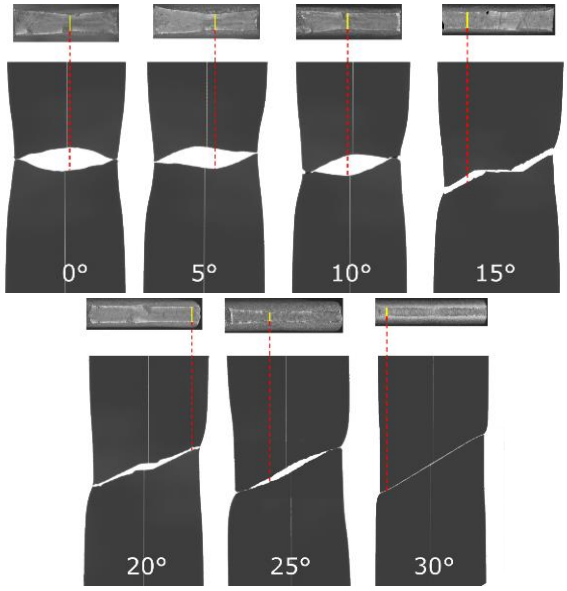

Fig. 1. Broken samples parts matched and minimum thickness location vs. fracture angle.

2.2 Cracks near samples shoulder radius

Cracks too close to the sample shoulder radius - although non-common - are illustrated in Fig. 2.

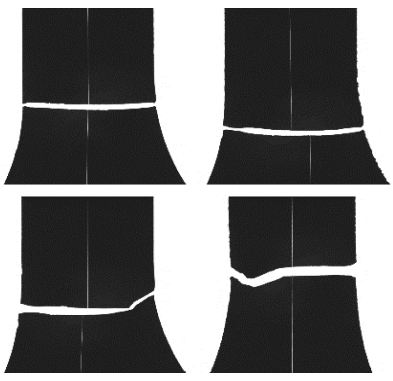

Fig. 2. Sample shoulder crack formation examples.

Such atypical failures jeopardize local ductility values since necking cannot properly unfold, leading to premature failure. Those invalid tests should be addressed in future VDA 238-110 standard revisions.

2.3 Edge cracks

Edge cracks are best revealed when virtually joining both broken sample parts after testing as shown in Fig. 3. Broken sample parts barely match with cracks starting normal to the tensile direction, typically without significant necking and an asymmetric fracture shape pattern [13]. Such tests are considered invalid for bulk material local ductility measurement. This should be also clarified in next VDA 238-110 revisions.

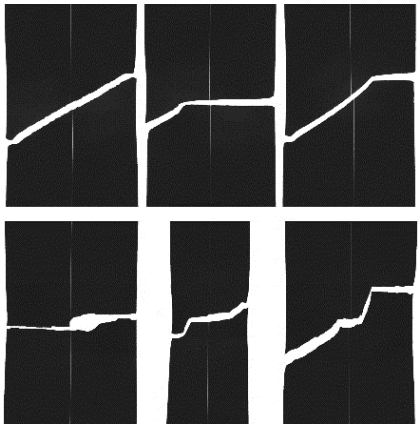

Fig. 3. Sample edge cracks formation examples.

2.4 Edge breakouts in width direction

Fig. 4 shows the correspondence between side and front view of broken samples to better identify the real fracture shape borders.

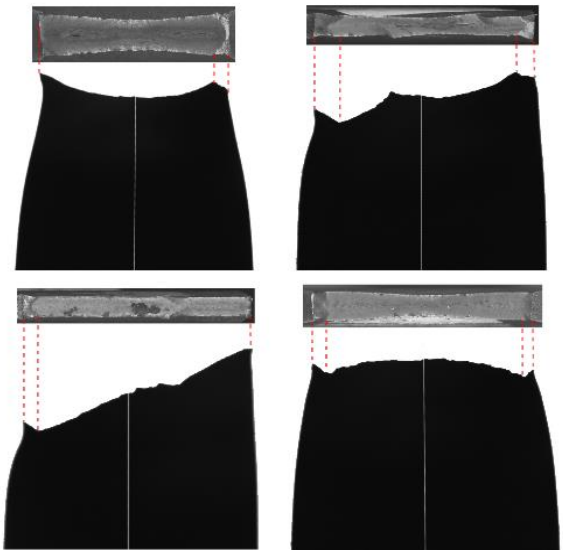

Fig. 4. Edge breakout examples side vs. front sample view.

Looking at the front view fracture shape under the microscope, it is not always obvious, where the left or right edge of fracture region lies. The edge of fracture region may then be wrongly determined, which leads to false values for reduction of area and/or minimum thickness values. Breakouts are best seen in the corresponding side view fracture shape (Fig. 4).

2.5 Thickness definition at samples edges

Fig. 5 illustrates the ambiguity of thickness definition close to sample edges. The thickness is defined as the cross section of a vertical line with the sample fracture contourplot. If this line crosses "empty air" at samples left/right outer edges, then the thickness is actually not properly defined (red line segments in Fig. 5). A stricter definition of sample edges is therefore proposed in Fig. 6. The farthest point C away from corners points A and B in horizontal direction along the lateral edge curve is determined. The corresponding dotted red line is then defined as the ultimate vertical edge of the sample (Fig. 6). The same principle applies for the horizontal upper/lower ultimate edges using cross-section lines in width direction with points E and F in Fig. 7. More accurately defined sample fracture edges limits reduce outliers especially in thickness t_{min} measurements. This should be a future revision point for VDA238-110.

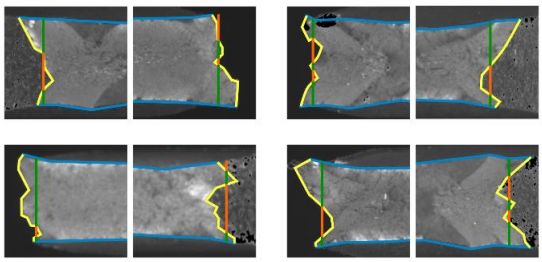

Fig. 5. Undefined thickness definition at samples edges.

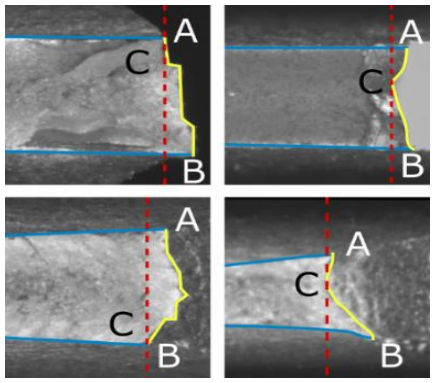

Fig. 6. Sample corrected edge definition range.

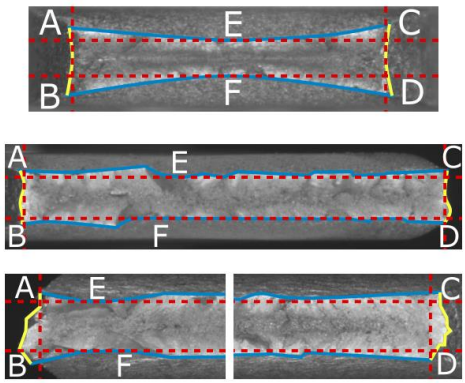

Fig. 7. Corrected upper/lower & right/left edge definition.

2.6 Thickness measurement error

Fig. 8 and Fig. 9 illustrate the error range when dealing with minimum thickness measures as prescribed in the VDA 238-110 test specification [1]. Local outbreaks in fracture shape severely affect the thickness measurement accuracy, leaving excessive room for subjectivity (Fig. 8). Both broken parts do not yield exact symmetric numerical values for individual thickness measurements with at least ±5µm measurement scatter for a specific location (Fig. 9). Especially rectangular shaped fractures at high fracture angle are challenging, requiring many measurements to cross-check the exact location and value of minimum thickness with poor reproducibility and repeatability. The thickness in mm can only be given seriously with 2 significant decimal digits, i.e. ±10-20µm measurement error at least, meaning ±1-2% relative error for 1mm thickness for example. Decimal digits in numerical values of derived % thickness or area reduction at fracture are therefore actually meaningless.

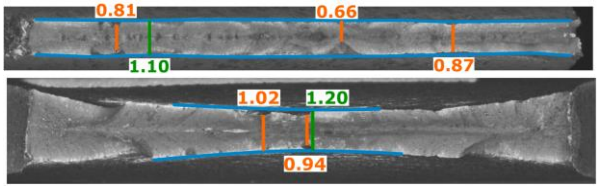

Fig. 8. Minimum thickness breakout related subjectivity.

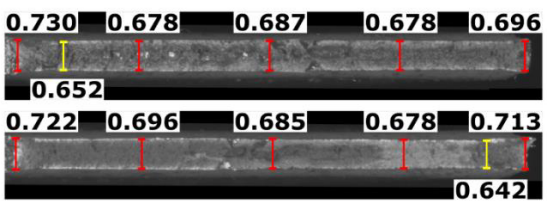

Fig. 9. Thickness measured from both broken sample parts.

3 Influence of sample geometry

Two typical cold rolled GI grades DP800 and CP1000 have been selected in the thickness range 1.0, 1.6, 2.2 mm for DP800 and 1.0, 1.5, 2.2 mm for CP1000. Different standardized tensile sample geometries with 7.5, 12.5, 20 and 25mm width have been tested with 3 replicates in longitudinal (L) and transverse (T) directions. This results in a broad width-to-thickness ratio (w/t) range between 3 and 25.

A classification for percentage of V-Type within each fracture surface has been performed. The S-Type (45° shear slant fracture in thickness direction) is identified under microscope, and the V-Type proportion across sample fracture width, also named Ductile Normale Fracture %DNF, is then deduced as the complementary value to 100% (%DNF=%V=100-%S). More details on this method are given in [1, 11].

3.1 Fracture angle vs. w/t ratio

Fig. 10 to Fig. 13 show the tanh Charpy-like dependency of fracture angle vs. w/t ratio for DP800 and CP1000. The higher the w/t ratio, the higher the fracture angle. This dependency is however highly non-linear with a steep transition at w/t=8.5±1.5 for DP800 and even steeper at w/t=5±1 for CP1000. The maximum fracture angle reaches ≈25° for DP800 and ≈30° for CP1000.

The tanh fitting between upper and lower fracture angle levels is performed as described in [10]. There is

therefore a direct analytical function translating fracture angle and the w/t sample geometry parameter. The width reduction is also linked analytically to the w/t parameter and can be actually accurately modelled as a function of material work hardening and sample geometry (w/t). The fracture morphology expressed as %DNF fracture type is plotted in Fig. 11 and Fig. 13. Small fracture angles in the lower w/t region correspond to a shear slant fracture mode with low DNF values.

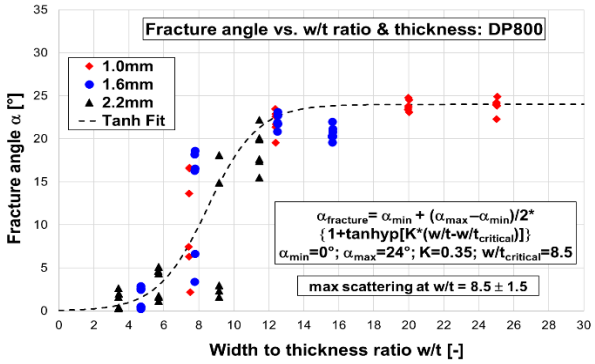

Fig. 10. Fracture angle vs. w/t and thickness, DP800 (L+T).

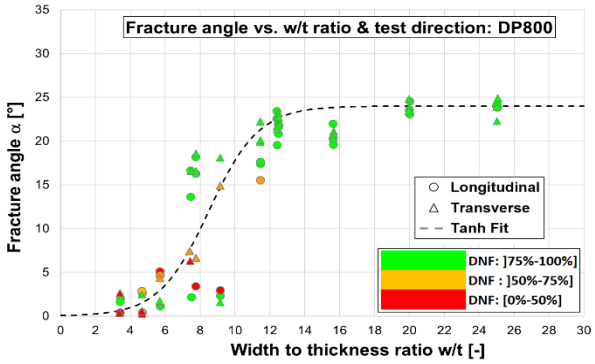

Fig. 11. Fracture angle vs. w/t, direction & DNF, DP800.

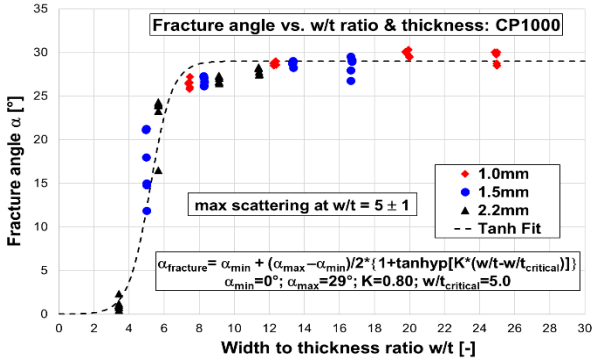

Fig. 12. Fracture angle vs. w/t and thickness, CP1000 (L+T).

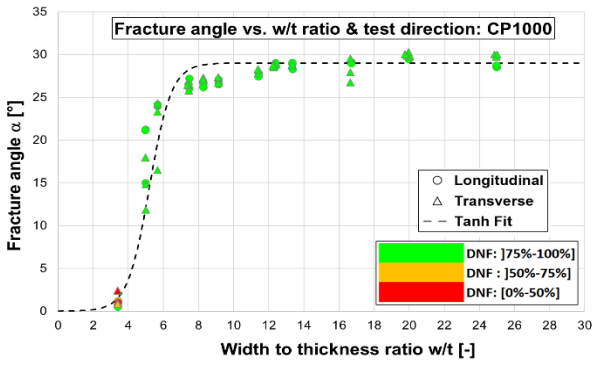

Fig. 13. Fracture angle vs. w/t, direction & DNF, CP1000.

3.2 %width reduction at fracture vs. w/t ratio

The w/t dependency of % width reduction is shown in Fig. 14 and Fig. 15 for DP800 and CP1000 respectively. It can be analytically described quite accurately with a simple power law. The narrower the sample, the more necking occurs in width direction under dominant uniaxial strain path condition [5]. Narrow sub-size ASTM-like (w=7.5 mm) tensile samples follow the uniaxial strain path up to fracture more closely, while wider JIS tensile samples (w=25 mm) on the contrary show more of a plane strain behavior (less width reduction) beyond uniform elongation.

This is actually very similar to forming limit diagram experimental methodology with FLD samples: 20-30 mm wide FLD samples drift toward uniaxial strain path while 70-110 mm broader samples are used for plane strain FLD_0 determination. The w/t dependency of tensile fracture width reduction is more pronounced for low n-value CP1000 (Fig. 15) than for DP800 (Fig. 14) with higher work hardening ability.

The w/t dependency of fracture width reduction can be depicted as shown in Fig. 14 and Fig. 15 with FE-simulations (ABAQUS/Explicit anisotropic elasto-plastic simulation - Hill48 - using volumetric elements). It is therefore more of a plasticity related global ductility property up to localized necking. The deformation is frozen in width direction as soon as local necking is concentrated in shear bands (Fig. 16). This effect is mostly relevant for the w/t dependency of the % reduction of area at fracture, which contains both thickness and width reduction contributions.

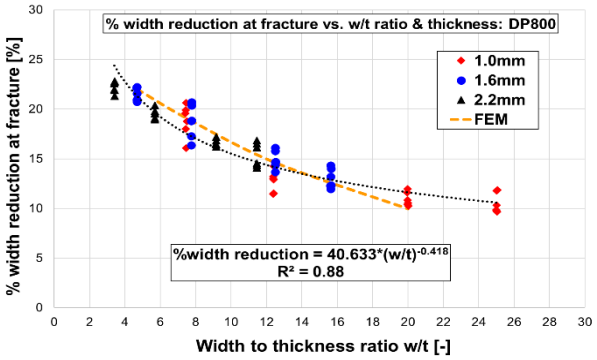

Fig. 14. % width reduction vs. w/t & thickness, DP800 (L+T).

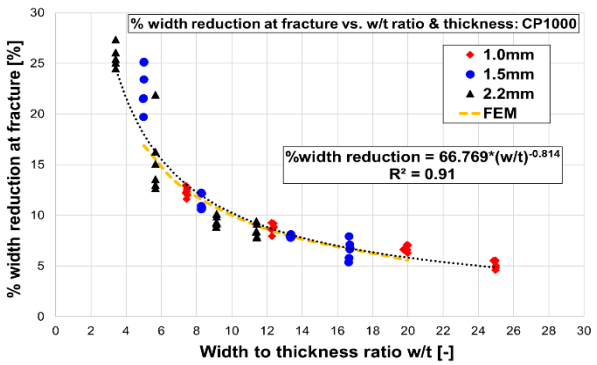

Fig. 15. % width reduction vs. w/t & thickness, CP1000 (L+T).

At high fracture angles, all deformation during post-uniform localized necking concentrates in shear bands, leaving triangular shaped undeformed "frozen zones"

with a characteristic straight outer edge, accompanied by an overall sample lateral shear motion (Fig. 16, [10]).

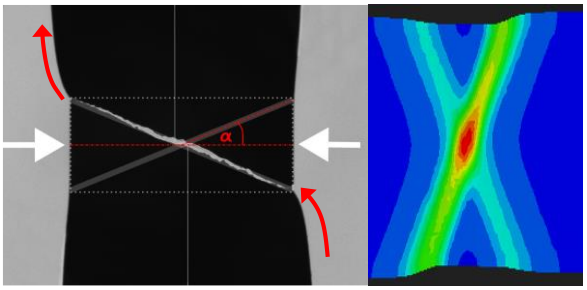

Fig. 16. Localized necking and sample shear band twisting.

3.3 Local ductility vs. w/t ratio

The reduction of area (Fig. 17, Fig. 18) as well as thickness reduction at minimum thickness (Fig. 19, Fig. 20) have been determined according to VDA 238-110 with additional DNF values. It is obvious that two separate local fracture strain levels coexist. One at low w/t in a ductile shear slant fracture dominant mode and another at high w/t in ductile normal cup & cone fracture mode. This is the case not only for area reduction but also for the thickness reduction at t_{min}.

A given testing geometry may inevitably end up within the high scattering transition range between upper (normal) and lower (shear) ductile local ductility level. In the stable upper and lower level, the scattering is quite low. In the transition range the scattering is stochastic and broad, impacting local ductility values.

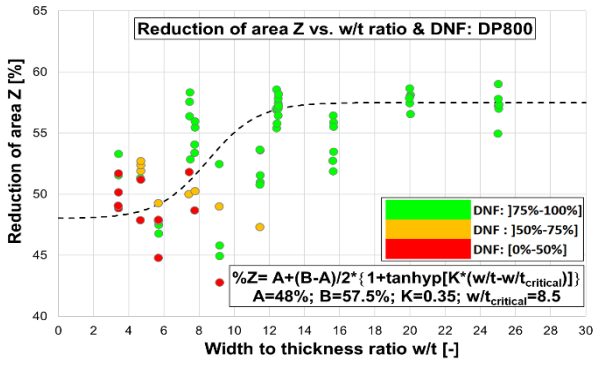

Fig. 17. % Reduction of area vs. w/t & DNF, DP800 (L+T).

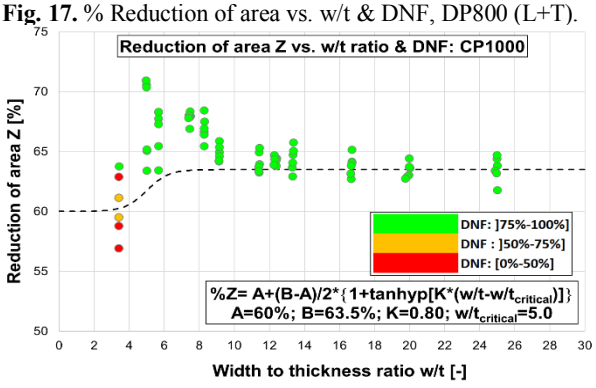

Fig. 18. % Reduction of area vs. w/t & DNF, CP1000 (L+T).

The transition w/t range also sees a sudden unexpected jump in both area and thickness at t_{min} reduction for CP1000 (Fig. 18, Fig. 20). The information about fracture mode or indirectly about fracture angle is therefore quite important for results interpretation. Critical w/t regions around 7-10 for DP800 and 4-6 for CP1000 should be avoided.

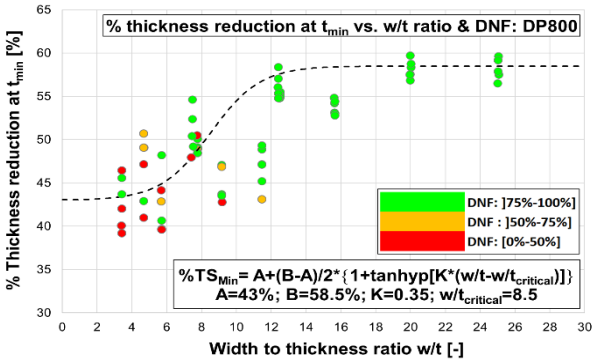

Fig. 19. % thickness red. at t_{min} vs. w/t & DNF, DP800 (L+T).

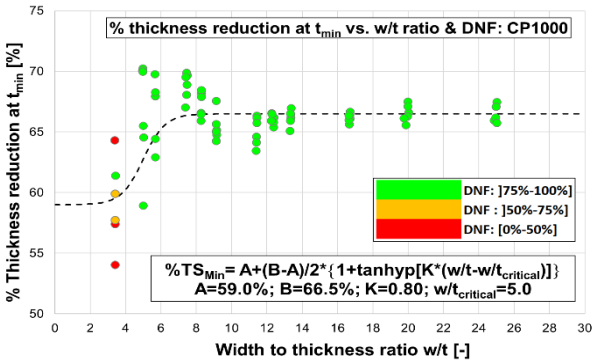

Fig. 20. % thickness red. at t_{min} vs. w/t & DNF, CP1000 (L+T).

3.4 FFL-FLC formability plots vs. w/t ratio

Following the concept of Forming Fracture Line introduced in [19] is a promising way for generalized local formability assessment in the minor-major strain usual FLC space. The True Fracture Strain derived from area reduction (major strain) is plotted against the true logarithmic width reduction at fracture (minor strain) from tensile samples fracture area microscope measurements as proposed in [5]. Fig. 21 and Fig. 22 show all results gathered for DP800 and CP1000.

The constant thinning lines are plotted and the FFL_0 cross section to the Y-axis of both upper (ductile normal) and lower ductility levels (ductile shear fracture level) are determined similar to FLC_0. The postuniform ductility beyond FLC is then expressed by the quantities FFL_0-FLC_0 or FFL_0/FLC_0 or $(FFL_0\text{-}FLC_0)/FLC_0$ in % as shown in Table 1. The superior postuniform ductility of CP1000 is shown hereby in comparison to DP800.

The wide variety of tensile geometries mixes both strain path (triaxiality) as well as fracture type (ductile normal cup&cone vs. ductile shear slant fracture type), which severely complicates the results interpretation. The lower w/t samples drift in pure uniaxial tensile mode but at the same time in the worst-case shear type modus. The high w/t samples reflect rather a plane strain condition in the best-case ductile cup&cone mode. The fracture type should be therefore indicated for a fair material comparison. In fact the data give some rough calibration points of the FFL curve in the uniaxial-plane strain triaxiality region with an additional distinction between ductile normal and ductile shear fracture modes according to the CrachFEM methodology [20, 21].

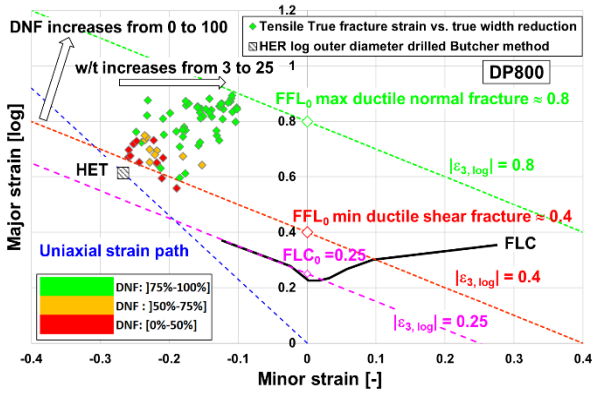

Fig. 21. $FFL_{tensile}$ - FLC ductility plot vs. w/t, DP800 (L+T).

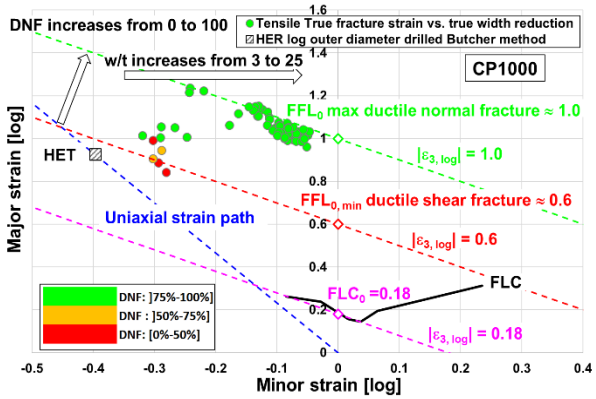

Fig. 22. $FFL_{tensile}$ - FLC ductility plot vs. w/t, CP1000 (L+T).

Table 1. Postuniform ductility derived from FFL_0 vs. FLC_0.

Material	FLC_0	FFL_0 max	FFL_0 / FLC_0	(FFL_0 - FLC_0)/ FLC_0
	-	-	-	%
DP800	0.25	0.8	3.2	220
CP1000	0.18	1.0	5.6	456

4 Conclusions

The flat sheet local ductility determination based on microscope measurements makes sense as a counterpart to round bar tensile samples. It delivers the zero-gage length true fracture elongation as opposed to the A_{xx} conventional total elongation. This is a true material property, which is at last available for flat sheet samples. From a testing and physical point of view both minimum thickness as well as reduction of area at fracture are considered as equally meaningful measures.

Some testing issues are still pending when dealing with local irregularities in fracture shape (edge definitions, breakouts in width and thickness direction, edge cracks, cracks too close to sample shoulder radii). Pure experimental (absolute) measurement errors on % reduction of thickness & area are in the order of at the very least ±1-2 %. Sample geometry effects (width to thickness ratio, fracture angle variations) mean however some much greater systematic absolute differences of up to 10-15 %! for both values.

Sorting out results according to shear vs. ductile fracture type or vs. sample fracture angle and w/t ratio is therefore a necessity when dealing with local tensile ductility measures. Such geometric effects are much more significant for local ductility properties than for usual A_{xx} total elongation.

This w/t dependency for local ductility properties severely complicates the use of local ductility values for industrial use with conventional tensile tests. Local ductility properties can only be properly interpretated with at least additional w/t and fracture angle information. Similar issues are faced for example with proportional and non-proportional flat sheet samples A_5 to A_{xx} fracture elongation conversions.

References

1. VDA 238-110 Test specification: Determination of Local Ductility by Fracture Surface Analyses of Tensile Test Specimens (08/2023)
2. R. Lingbeek, P. Larour, A. Ruck, T. Beier, S. Westhäuser, Mater. Res. Proc. **41,** 999 (2024)
3. WorldAutoSteel AHSS Guidelines https://ahss insights.org/forming/formability/true-fracture-strain/
4. B. Hance, SAE Int.J.Mater.Manf. **11**(4), 505 (2018)
5. B. Hance, T.Link, Mater.Sci.Eng. **651** 012061(2019)
6. G. Yim, J. Kim, J. Jeon, J. Hyun, B. Hance, Mater. Sci. Eng. **1307** 012015 (2024)
7. B. Hance, SAE Int. J. Engines **10**(2), 247 (2017)
8. M. Gruenbaum, G. Aydin, T. Dettinger, S. Heibel, Mater.Sci.Eng. **651** 012056 (2019)
9. L. Wagner, Mater. Sci. Eng. **418** 012074 (2018)
10. P. Larour, L. Wagner, A. Felbinger, J. Angeli, Mater. Sci. Eng. **651** 012016 (2019)
11. L. Wagner, P. Larour, F. Sonnleitner, A. Felbinger, J. Angeli, Mater. Sci. Eng. **1157** 012045 (2021)
12. P. Larour, J. Freudenthaler, M. Kerschbaum, D. Dolzer, Mater. Sci. Eng. **967** 012080 (2020)
13. P. Larour, J. Freudenthaler, H. Pauli, J. Angeli, Mater. Sci. Eng. **1157** 012054 (2021)
14. J. Hu, G. Thomas, C. Campbell, SAE Int.J. Advan ces & Curr. Prac. in Mobility **4**(4), 1394 (2022)
15. J. Hu, On True Fracture Strain (TFS) of AHSS Sheets: Measurement and Derivation. 21st Great Designs in Steel GDIS Conf., Novi, USA (2023)
16. I.A. Denks, M. Schneider, S. Westhäuser, C. Lesch, Steel Research Int. **90** (6) 1800460 (2019)
17. P. Plosila, V. Kesti, J. Hannula, A. Kaijalainen, Mater. Today Commun., **40** 109521 (2024)
18. W. Cho, B.S. Jeong, K. Jeong, S.H. Lee, H.N. Han, J. Mater. Res. Technol. **26**, 837 (2023)
19. P.A.F. Martins, N. Bay, A.E. Tekkaya, A.G. Atkins, Int. J. Mech. Sci. **83** 112 (2014)
20. L. Kessler, T. Beier, H. Werner, D. Horstkott, H. Dell, H. Gese, Material Selection for an UHSS Component Based on the Failure Criteria of CrachFEM, AIP Conf. Proc. **778**, 492 (2005)
21. H. Dell, H. Gese, G. Oberhofer, CrachFEM–A Comprehensive Approach For The Prediction Of Sheet Metal Failure. AIP conf. proc. **908** (2007)